A comparative study on long and short carbon nanotubes-incorporated polypyrrole/poly(sodium 4-styrenesulfonate) nanocomposites as high-performance supercapacitor electrodes

Haihan Zhou*, Gaoyi Han*, Yaoming Xiao, Yunzhen Chang, Hua-Jin Zhai

Institute of Molecular Science, Key Laboratory of Materials for Energy Conversion and Storage of Shanxi Province, Key Laboratory of Chemical Biology and Molecular Engineering of Education Ministry, Shanxi University, Taiyuan 030006, China

ABSTRACT

Polypyrrole/poly(sodium 4-styrenesulfonate)-carbon nanotubes (PPy/PSS-CNT) nanocomposites have been fabricated with an in situ electrochemically polymerized method. The long (10–30 μm) and short (0.5–2 μm) CNT are incorporated separately into the composites, and their effect on the capacitive performance of composites prepared is compared. Scanning electron microscope characterization reveals that long CNT-incorporated composites (PPy/PSS-lCNT) have the more porous microstructure and present a large amount of CNT within the composites, in which these long tangled CNT form an interconnected conductive nano-network. Furthermore, combining with the transmission electron microscopy characterization, both of the two types of composites show the core–shell nanostructure with PPy layer coated on CNT. The results by electrochemical tests including cyclic voltammetry (CV), galvanostatic charge/discharge (GCD), and electrochemical impedance spectroscopy (EIS) manifest the PPy/PSS-lCNT composite electrodes have the relatively more superior capacitive behavior and cycle stability than those of the short CNT-incorporated composites (PPy/PSS-sCNT) electrodes. Thereinto, the PPy/PSS-lCNT composite electrodes exhibit a high areal capacitance of 146.1 mF cm^{-2} at 10 mV s^{-1} CV scan, retaining 94.0% of the initial capacitance after 5000CV cycles. This comparative study suggests that the long CNT-incorporated PPy/PSS-lCNT nanocomposites are relatively more promising as the electrode materials for the high-performance supercapacitors.

© 2015 Elsevier B.V. All rights reserved.

1. Introduction

Nowadays, it is a major challenge for researchers to provide environmentally friendly, low-cost, and high-efficient electrical devices for energy storage, addressing the approaching problems of climate change and exhaustion of fossils fuels. As a promising energy-storage device, supercapacitors (also called electrochemical capacitors) have attracted considerable attention in power sources applications due to their higher power density and longer cycle life than secondary batteries and higher energy density compared to conventional capacitors, and they are applicable in portable electronics, uninterruptible power sources, electric vehicles, and renewable energy sources [1–7].

The electrode material is a key factor to affect the performance of supercapacitors, and recent research efforts have been focused on improving the energy density of supercapacitors by exploring novel electrode materials [8–10]. The energy storage can be divided into two types, one is caused by the adsorption of ions onto the electrodes, which is called electrical double-layer capacitance, the other is stored through reversible redox reactions at the electrodes, which is referred to as pseudocapacitance because it behaves electrically as a capacitance, although the reactions of charge transfer are more like a battery [11–13]. The electrode materials with electrical double-layer capacitance are mainly carbon materials such as activated carbon, graphite, graphene, and carbon nanotubes etc., among them, carbon nanotubes (CNT) have been extensively investigated due to their nano-scale texture and superior properties including large surface area, high electrical conductivity, chemical stability, and low-cost [14,15]. The electrode materials based on pseudocapacitance commonly contain transitional metal oxides and conducting polymers. Thereinto, conducting polymers show the advantages of high inherent conductivity, ease and versatility in synthesis, and low cost compared with metal oxides [16,17]. Polypyrrole (PPy), one of most studied conducting polymers, possesses high electrical conductivity, large

* Corresponding authors. Fax: +86 351 7016358.
E-mail addresses: hhzhou@sxu.edu.cn (H. Zhou), han_gaoyis@sxu.edu.cn (G. Han).

specific capacitance, chemical stability, and cost effectiveness [18,19]. Commonly, carbon nanotubes (CNT) have high power density and good cycle life but low capacitance, PPy possesses high energy density but a low cycle life due to that swelling and shrinkage may occur in the process of doping/dedoping [20,21]. Based on the complementary properties of CNT and PPy, considerable efforts have been devoted to exploring hybrids of CNT and PPy to obtain high-performance electrode materials [22–25]. However, these studies usually use the methods of chemical oxidative polymerization or complicated multiple-step procedures. Compared with the chemical oxidative polymerization, electrochemical polymerization have the advantages like that the composite films can be directly coated on the electrode substrates, the thickness of films can be controlled easily, and the films are free from impurities such as the oxidant and its reaction products. In addition, since the weak solubility and dispersity of CNT remain the hinder to obtain the high-performance composite electrode materials, especially in our preliminary experiment, we found the solution for electrochemical polymerization nearby the electrode substrates with large area would become clear as a result of that CNT would be consumed completely when only the PPy and CNT are present. Based on it, poly(sodium 4-styrenesulfonate) (PSS) polyelectrolyte will be added into the solution for electrochemical polymerization to improve the solubility and dispersity of CNT, and a one-step electrochemically polymerized method will be used to fabricate the PPy/PSS-CNT composite electrodes. In addition, up to now, no research focuses on the effect of different types of CNT on the capacitive performance of composites consist of CNT and PPy, here we will emphasize comparing the effect of long and short CNT on the capacitive performance of composites.

In this research, the long and short CNT are incorporated separately into the composites (PPy/PPS-lCNT and PPy/PPS-sCNT) with an in situ electrochemically polymerized method. The compositions and morphology of the composites were studied using Fourier transform infrared spectroscopy (FT-IR), scanning electron microscope (SEM), and transmission electron microscopy (TEM). The electrochemical characteristics of electrode prepared were investigated with cyclic voltammetry (CV), galvanostatic charge/discharge (GCD) measurements, and electrochemical impedance spectroscopy (EIS). The effect of long and short CNT on the capacitive performance of composites prepared is compared detailedly.

2. Experimental

2.1. Reagents and materials

Pyrrole (99%) was purchased from Aladdin Chemistry Co., Ltd., long and short carboxylic multi-wall carbon nanotubes (lCNT-COOH and sCNT-COOH) were supplied by Chengdu Organic Chemicals Co., Ltd., their length was 10–30 μm and 0.5–2 μm, respectively, which were the longest and shortest CNT-COOH they could supply, both of their outer diameter was <8 nm, and their making method was chemical vapor deposition (CVD). Poly (sodium 4-styrenesulfonate) (M.W. = 70,000) was obtained from

Alfa Aesar. Fluorine-doped tin oxide (FTO, 8 Ω/□) conducting glasses were purchased from Dalian Heptachroma SolarTech, before use, conductive areas (1 cm×1 cm) were exposed with adhesive tape as the electrode substrate for electrochemical polymerization.

2.2. Preparation of PPy/PSS-CNT nanocomposites electrodes

The PPy/PSS-CNT nanocomposites electrodes were prepared with an in situ electrochemically polymerized/deposited method (left, Fig. 1). In this study, the FTO conducting glasses were chosen as the substrate for electrodepositon due to their high conductivity and they are also commonly used as the conductive substrate for the dye-sensitised solar cells (DSSCs). Prior to electrochemical deposition, the FTO conducting glasses were ultrasonically cleaned with acetone and deionized water successively. After that, the cleaned conducting glass was fixed in a two-electrode cell with a large-area Pt sheet serving as the counter electrode and pseudo-reference electrode. An aqueous solution consists of 0.25 M pyrrole momomer, 0.01 M PSS, and 2 mg/ml sCNT-COOH (or lCNT-COOH) was used as the deposition solution, in which the PSS acts as supporting electrolytes as well as dopants. Before use, the deposition solution was dispersed under ultrasonication for about 20 min, subsequently the electrochemical deposition was performed with a galvanostatic mode, to avoid the overoxidation of pyrrole, a low constant current density of 1.0 mA cm^{-2} was used for 30 min. The electrodes prepared with the long and short CNT were denoted as PPy/PSS-sCNT and PPy/PSS-lCNT eletrodes, respectively. As a comparison, the PPy/PSS electrodes were fabricated from an aqueous solution containing 0.25 M pyrrole and 0.01 M PSS with the same electrodeposition procedure. These films were grown with a total charge of 1.8 C cm^{-2} passed during polymerization, which was kept the same for all films prepared, in an attempt to keep the mass of films deposited identical. In addition, the pure PPy was likewise prepared from an aqueous solution containing 0.25 M pyrrole monomer and 1 M KCl for the FT-IR test.

2.3. Composition and morphology characterizations

FT-IR spectra were recorded by using a Bruker Tensor 27 FT-IR Spectrometer. The test samples were scraped from the electrode substrates and prepared with KBr tabletting. The surface morphology of PPy/PSS, PPy/PSS-sCNT, and PPy/PSS-lCNT films were observed with a filed emission scanning electron microscope (JSM-6701F, JEOL) operating at 10.0 kV, the samples were sputtered with platinum before observation. The TEM images of PPy/PSS-sCNT and PPy/PSS-lCNT composites were obtained using a high resolution transmission electron microscopy (JEM-2100, JEOL) operated with a voltage of 200 kV.

2.4. Electrochemical measurements

The electrochemical measurements were performed on a CHI 660B electrochemical workstation (Chenhua, China) with two-electrode
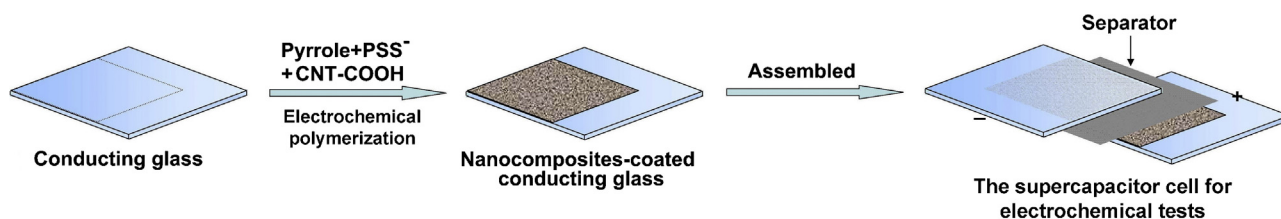
Fig. 1. The schematic diagram for the electrochemical polymerization of PPy/PSS-CNT nanocomposites and the supercapacitor cell assembled by two pieces of symmetric nanocomposites-coated conducting glasses for electrochemical tests.

system. The sandwich-like supercapacitor cell for tests was assembled with two pieces of identical films-deposited FTO conducting glass electrodes, in which one was oxidized and the other reduced (right, Fig. 1). A piece of filter paper soaked with 1 M KCl solution was used as the separator, the conducting glass itself served as the current collector. The CV measurements were carried out in a potential range of −0.5 to 0.5 V at varying scan rates. The GCD tests were performed at varying current densities between potentials of −0.5 to 0.5 V. The EIS were measured at the open-circuit potential and the data were recorded in the frequency range from 100 k to 0.01 Hz using AC-voltage amplitude of 5 mV. In order to ensure the accuracy of the data reported, four parallel supercapacitor cells were tested for each sample.

With the purpose of the applications like stationary energy storage devices and small scale electronics, it is a better indicator to depict supercapacitor performance using areal capacitance compared with mass specific capacitance [26,27], so this research focuses on the areal capacitance of electrodes. The areal capacitance (C_s) of the single electrode can be calculated from the CV curves according to the Eq. (1):

$$C_s = \frac{\int i \mathrm{dV}}{S \times \Delta V \times \nu} \tag{1}$$

thereinto, C_s is the areal capacitance ($F\,cm^{-2}$), $\int i \mathrm{dV}$ the integrated area for the CV curve, S the surface area of active materials in the single electrode (cm^2) and fixed at $1\,cm^2$ in this research, ΔV the scanning potential window in V and ν the scan rate in $V\,s^{-1}$.

Based on the galvanostatic charge/discharge curves, the areal capacitance of the single electrode can be obtained with the Eq. (2):

$$C_s = \frac{2 \times i \times t}{S \times \Delta V} \tag{2}$$

here C_s is the areal capacitance ($F\,cm^{-2}$), i the discharge current (A), t the discharge time (s), S the surface area of the active materials on the single electrode (cm^2) and fixed at $1\,cm^2$ in this research, ΔV the scanning potential window (V).

The areal energy density and power density of the single electrode shown in the Ragone plot can be calculated by the Eqs. (3) and (4), respectively.

$$E = \frac{\frac{1}{2}C_s \Delta V^2}{3600} \tag{3}$$

$$P = \frac{3600E}{t} \tag{4}$$

where E is the areal energy density ($Wh\,cm^{-2}$), P the areal power density ($W\,cm^{-2}$), C_s the areal capacitance ($F\,cm^{-2}$), ΔV the potential window subtracting iR drop (V) and t the discharge time (s).

3. Results and discussion

3.1. Composition analysis

During the preparation of composites, the carboxylic CNT and anionic PSS simultaneously served as the counter-ions for the polymerization of EDOT monomer. Fig. 2 shows the FT-IR spectra of sCNT-COOH, lCNT-COOH, PPy, PPy/PSS-sCNT, and PPy/PSS-lCNT, the peak located at 1722 cm^{-1} in sCNT-COOH and lCNT-COOH spectra can be attributed to the C=O stretching vibration of the —COOH [28]. For the PPy spectrum, the peaks at 1457 and 1540 cm^{-1} are designated as the stretching vibration of C—N and C—C in the pyrrole ring, respectively [29,30]. As expected, the
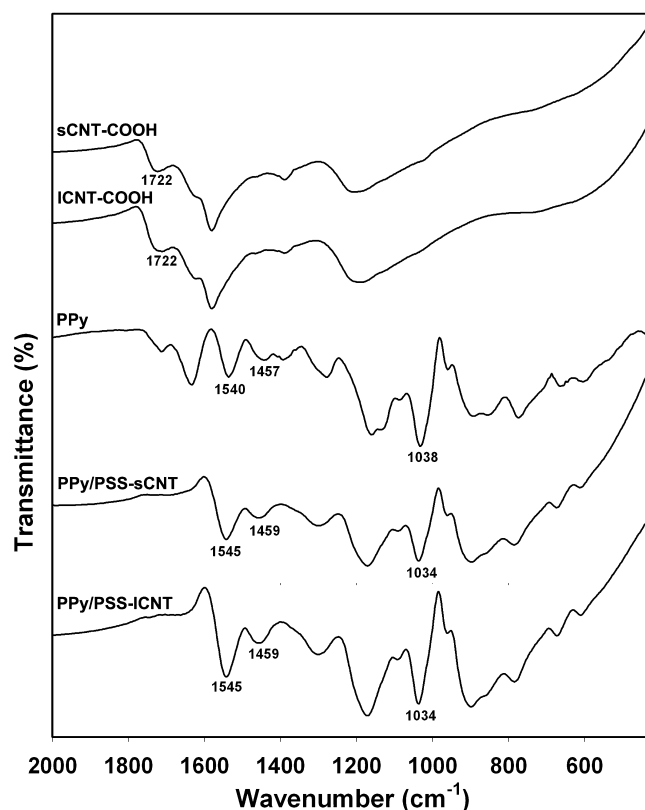
Fig. 2. FT-IR spectra of sCNT-COOH, lCNT-COOH, PPy, PPy/PSS-sCNT, and PPy/PSS-lCNT nanocomposites.

characteristic peaks at 1459 and 1545 cm^{-1} for PPy appear in the PPy/PSS-sCNT and PPy/PSS-lCNT composites, indicating the presence of PPy in the composites. It is also observed that the peak at 1038 cm^{-1} ascribed to the C—H in-plane vibration of PPy ring has shifted to 1034 cm^{-1} in the spectra of the two types of composites, which is caused by the electrostatic interaction originated from the PPy cations and the PSS anions as well as the incorporation of carboxylic CNT. In addition, the bands for carboxylic CNT are detected scarcely in the spectrum of composites probably due to they are too weak or overlapped by the peaks of PPy and PSS. The study by FT-IR spectra suggests the formation of PPy/PSS-sCNT and PPy/PSS-lCNT composites.

3.2. Morphology characterizations

The microstructure is an important feature for electrode materials applied in electrochemical capacitors. In this study, the length of long and short carboxylic CNT used is 10–30 μm and 0.5–2 μm, respectively. The thickness of PPy/PSS-sCNT and PPy/PSS-lCNT films is around 10 μm, and their mass is 0.82 and 0.85 mg, respectively. The PPy/PSS-lCNT films show the larger mass which may result in the higher surface specific capacity, however, it is probably more crucial for the microstructure and electroactive of the active materials to affect their capacitive properties. Fig. 3a exhibits the SEM images of PPy/PSS, PPy/PSS-sCNT, and PPy/PSS-lCNT composites at low (above) and high (below) magnification. It can be observed that the PPy/PSS films show a compact microstructure consists of some dense grains, which will be unfavorable to the access of electrolyte, consequently results in the inferior capacitive properties, and this will be testified in the following section. In contrast to PPy/PSS films, the PPy/PSS-sCNT and PPy/PSS-lCNT composite films display a very different surface morphology as the incorporation of CNT, we

(a)

(b)
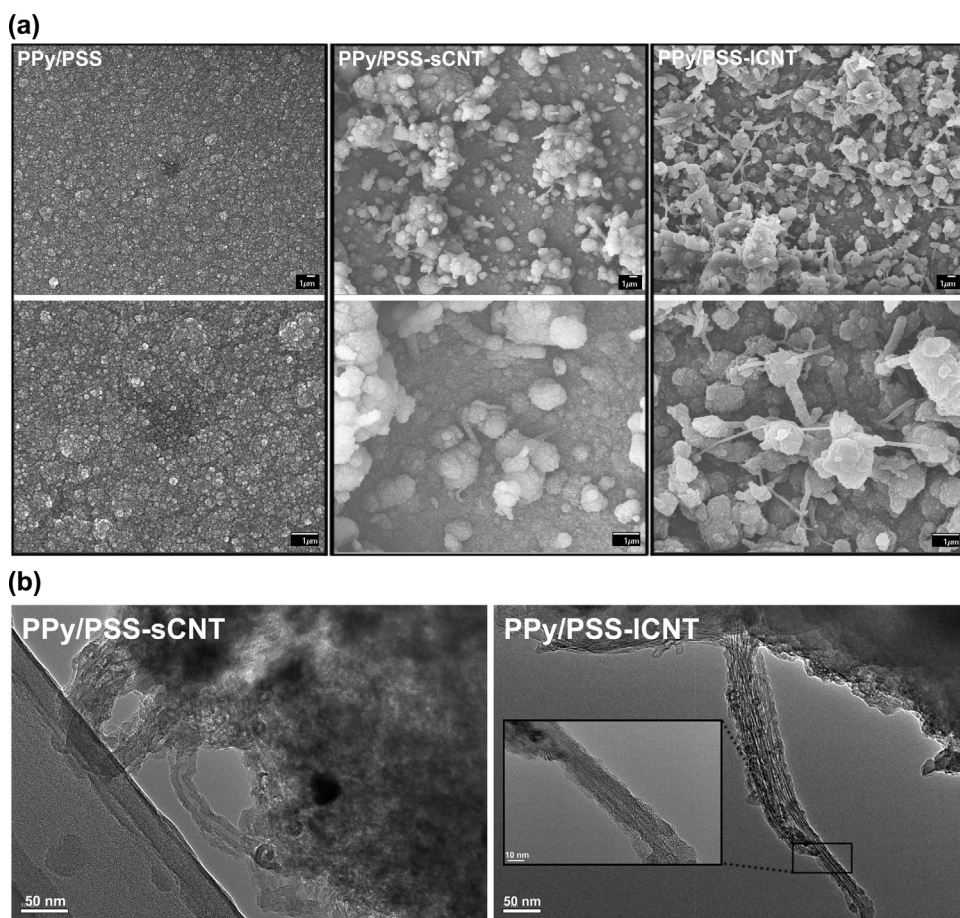
Fig. 3. (a) SEM images of PPy/PSS, PPy/PSS-sCNT, and PPy/PSS-lCNT nanocomposites with low (above) and high (below) magnification. (b) TEM images of PPy/PSS-sCNT and PPy/PSS-lCNT nanocomposites, the inset shows the partial magnified image.

can see that the two types of composites show a three-dimensional loose microstructure with the increased electro-active area. Furthermore, a careful observation for the two types of composites suggests the PPy/PSS-lCNT composites have the more loose and porous feature, this will enlarge the electrode/electrolyte interface and facilitate ion transfer from electrolyte within the composites. In particular, it can be clearly observed from the SEM images at high magnification, only a small amount of CNT appear in the PPy/PSS-sCNT composites, and these CNT are randomly scattered in the composites, probably due to these CNT are too short to form an interconnected network. On the contrary, PPy/PSS-lCNT presents the relatively more CNT within the composites, and these long tangled CNT form an interconnected conductive nano-network, these will effectively improve the charge transfer of composite films due to the high conductivity of CNT. In addition, it can be seen that the CNT in the two types of composites become thicker since the outer diameter of the as-received CNT was only <8 nm, the change in diameter is because the PPy layer coated on the CNT, consequently forms the core–shell nanostructure. Also the core–shell nanostructure can be further confirmed by the TEM images (Fig. 3b), for the two types of composites, the PPy/PSS polymers have encased bundles of CNT, and the CNT became thicker owing to coating with the PPy/PSS polymers. It should be noted that the core–shell microstructure formed can significantly reduce the ions diffusion distance and improve the charge transfer between
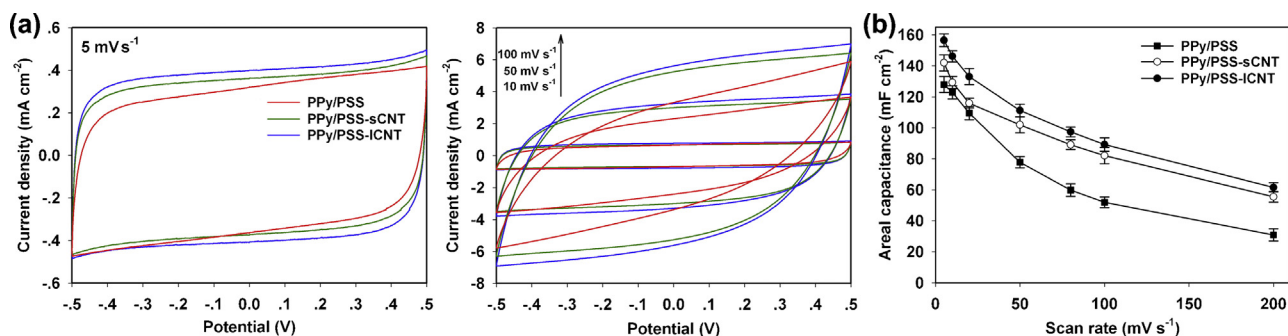
Fig. 4. (a) Cyclic voltammograms of the supercapacitor cells assembled by PPy/PSS, PPy/PSS-sCNT, and PPy/PSS-lCNT composite electrodes at varying scan rates of $5\,\mathrm{mV\,s^{-1}}$ (left) and $10–100\,\mathrm{mV\,s^{-1}}$ (right). (b) The relationship of areal capacitance versus scan rate for the PPy/PSS, PPy/PSS-sCNT, and PPy/PSS-lCNT composite electrodes. Data are presented as the mean ± standard error (SE) of the mean for types of electrodes ($n = 4$).

PPy/PSS and CNT, consequently leads to the promoted capacitive performance.

3.3. Electrochemical evaluation

3.3.1. Cyclic voltammetry

The CV curves of the supercapacitor cells assembled by PPy/PSS, PPy/PSS-sCNT, and PPy/PSS-lCNT composite electrodes at varying scan rates are shown in Fig. 4a. We can see from the 5 mV s^{-1} plots that the PPy/PSS-sCNT and PPy/PSS-lCNT electrodes exhibit more rectangular-like shape and larger CV area than those of PPy/PSS, and this trend become more obvious with the adding of scan rate (10–100 mV s^{-1}). It should be noted that the capacitor cells for CV tests are assembled with two pieces of identical electrode using two-electrode system, that one electrode is oxidized and the other reduced causes the unobvious oxidation/reduction peaks of PPy, consequently displays the rectangular CV shape [31]. Moreover, for PPy/PSS-sCNT and PPy/PSS-lCNT electrodes, the current obviously increased with adding scan rate, and the rectangular-like CV curves can be also observed at higher scan rates range from 10 to 100 mV s^{-1}, indicating that they have good rate capability. The above results manifest the capacitive performance of PPy-based electrodes are remarkably boosted as a result of the incorporation of CNT, this can be attributed that the incorporation of large anions CNT makes the composites less compact with large specific surface area, and the formed core–shell nanostructure effectively takes advantage of the Faradaic pseudocapacitance from PPy/PSS and electric double layer capacitance originated from CNT with high conductivity.

Fig. 4b exhibits the variation of areal capacitance with respect to CV scan rate for the three types of electrodes. PPy/PSS electrodes display the lowest areal capacitance in the whole scan rates. The areal capacitance of PPy/PSS electrodes is 127.9 mF cm^{-2} at 5 mV s^{-1} (122.9 mF cm^{-2} at 10 mV s^{-1}), while the areal capacitance of PPy/PSS-sCNT and PPy/PSS-lCNT electrodes increases to 142.0 and 156.5 mF cm^{-2} at 5 mV s^{-1} (129.2 and 146.1 mF cm^{-2} at 10 mV s^{-1}), respectively, which are higher than 25 mF cm^{-2} at 5 mV s^{-1} for PANI/graphite oxide composites and 64.6 mF cm^{-2} at 10 mV s^{-1} for TiO$_2$@PPy nanowires reported previously [32,33]. Furthermore, it can be seen that the long CNT-incorporated PPy/PSS-lCNT electrodes have the relatively higher capacitance value than that of short CNT-incorporated PPy/PSS-sCNT electrodes at all CV scan rates. The result indicates the long CNT can more effectively improve the capacitive performance of PPy/PSS-CNT composites, and this conclusion will be further discussed in the following section.

3.3.2. Galvanostatic charge/discharge measurements

In order to further compare the capacitive performance of PPy/PSS-sCNT and PPy/PSS-lCNT electrodes, the GCD measurements were also performed. Fig. 5a shows the GCD curves of supercapacitor cells assembled by PPy/PSS-sCNT and PPy/PSS-lCNT composite electrodes at the current density of 0.2 mA cm^{-2}. It can be observed from the plots that both of the two types of electrodes exhibit triangular-shape charge/discharge curves, but the PPy/PSS-lCNT electrodes show the relatively longer discharge time. Based on the GCD curves, the columbic efficiency (η) can be defined with the ratio of discharge time (t_d) to charge time (t_c). The η of PPy/PSS-lCNT electrodes is 96.7%, which is higher than 95.5% of PPy/PSS-sCNT electrodes at the GCD current density of 0.2 mA cm^{-2}. Fig. 5b shows the areal capacitance value of the two types of electrodes at varying current densities. At the current density of 0.2 mA cm^{-2}, the PPy/PSS-lCNT electrodes achieve the capacitance of 164.6 mF cm^{-2}, while the PPy/PSS-sCNT electrodes reveal 153.3 mF cm^{-2}. Furthermore, we can see that the PPy/PSS-lCNT electrodes display the relatively larger capacitance at all GCD
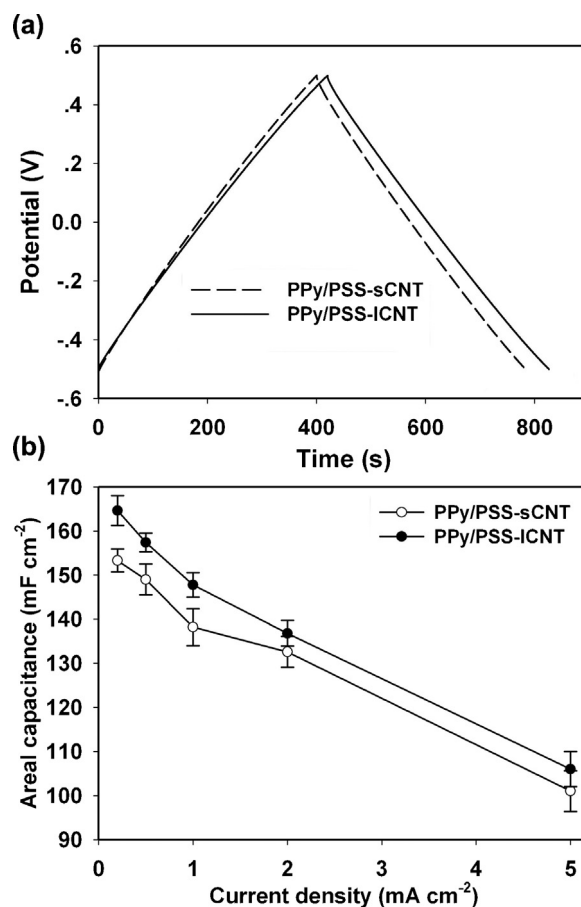
Fig. 5. (a) GCD curves of the supercapacitor cells assembled by PPy/PSS-sCNT and PPy/PSS-lCNT composite electrodes at the current density of 0.2 mA cm^{-2}. (b) The areal capacitance of PPy/PSS-sCNT and PPy/PSS-lCNT composite electrodes at different GCD current density. Data are shown as mean ± SE ($n = 4$).

current densities, which is in accordance with the results by CV tests. The GCD tests further indicate the long CNT can more effectively improve the capacitive performance of PPy/PSS-CNT composites. As shown in the SEM images, this can be ascribed to that PPy/PSS-lCNT composites show the more loose and porous feature and the presence of a large amount of CNT within the composites, besides these long tangled CNT form an interconnected conductive nano-network for more efficient charge transfer.

3.3.3. Electrochemical impedance spectroscopy

The EIS measurements were performed to further compare the electrochemical performance of PPy/PSS-sCNT and PPy/PSS-lCNT composite electrodes. The obtained complex plane EIS plots are shown in Fig. 6a, we can see that the impedance plots of the two types of electrodes display a feature of vertical trend at low frequencies, it is the capacitive behavior based on the equivalent circuit theory [34]. Compared with PPy/PSS-sCNT electrodes, the straight line in the low frequency for PPy/PSS-lCNT electrodes leans more towards imaginary axis, indicating the better capacitive character. It can be observed from the inset of Fig. 6a that there is no semicircle appears at high frequency region for the two types of electrodes, which is due to the low interfacial resistance of charge transfer [35]. In addition, also we can see from the inset of Fig. 6a that the intercept at x-axis for the impedance plot of PPy/PSS-lCNT electrodes is smaller than that of PPy/PSS-sCNT electrodes, manifesting the smaller equivalent series resistance (ESR). The ESR mainly originates from the electrolyte, the intrinsic resistance
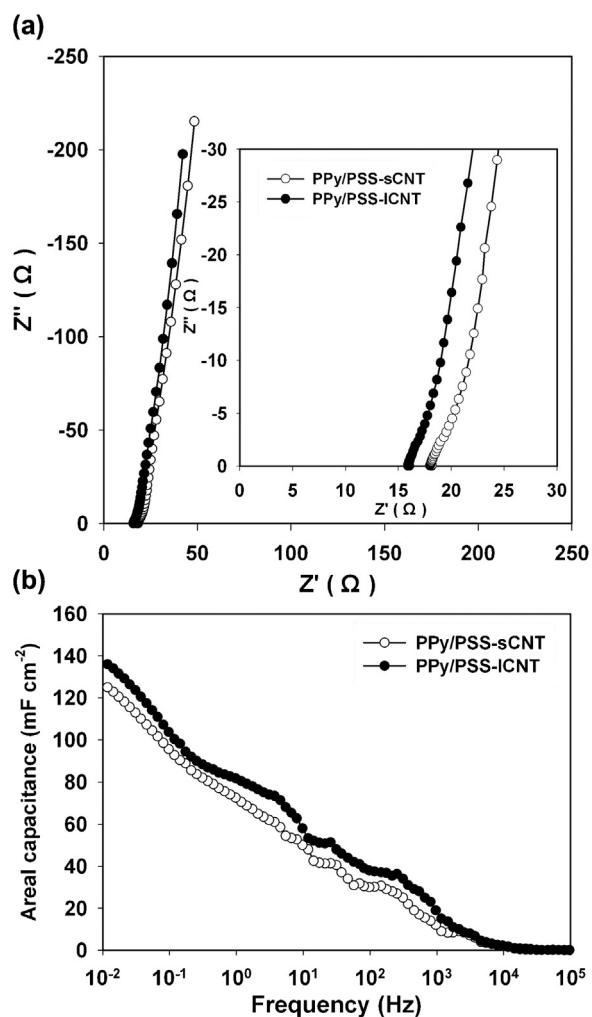
Fig. 6. (a) Complex plane EIS plots of the supercapacitor cells assembled by PPy/PSS-sCNT and PPy/PSS-lCNT composite electrodes, the inset shows the plots at high-frequency. (b) The plots of conversion areal capacitance versus frequency for PPy/PSS-sCNT and PPy/PSS-lCNT composite electrodes.

for electroactive materials, and the contact resistance at the active material/current collector interface [36].

Another important information can be obtained from the EIS is the conversion capacitance, the conversion capacitance can be calculated from the Eq. (5) [37]:

$$C_s = \frac{-1}{\pi S f Z''} \tag{5}$$

where C_s is the areal capacitance (F cm^{-2}), f the frequency (Hz), Z'' the imaginary part of EIS (Ω), and S the geometric surface area of electroactive materials on single electrode (1 cm^2 fixed in this research). Fig. 6b presents the plots of conversion capacitance vs. frequency for the two types of electrodes, we can see that the PPy/PSS-lCNT electrodes show the relatively higher areal capacitance at the whole frequency region, agreeing well with the CV and GCD test results.

3.3.4. Ragone plot and cycle stability

Fig. 7a presents the Ragone plots for PPy/PSS-sCNT and PPy/PSS-lCNT electrodes, we can observe that the PPy/PSS-lCNT electrodes reveal the higher energy and power densities than those of PPy/PSS-sCNT electrodes all the time. Thereinto, the PPy/PSS-lCNT electrodes deliver a power density of 198.5 μW cm^{-2} at energy density of
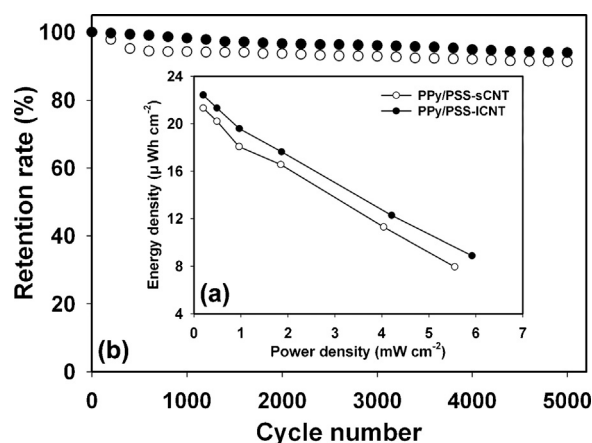
Fig. 7. (a) Ragone plots of PPy/PSS-sCNT and PPy/PSS-lCNT composite electrodes. (b) The relationship between capacitance retention rate and cycle number for stability tests of PPy/PSS-sCNT and PPy/PSS-lCNT composite electrodes at 100 mV s^{-1} CV scan.

22.4 μWh cm^{-2}, while it maintains 5920 μW cm^{-2} at 8.88 μWh cm^{-2}, exhibiting higher power density and energy density compared with conducting polymers reported previously [32,38]. The cycle stability is a significant character for the electrodes applied for supercapacitors, here a 5000CV cycles at 100 mV s^{-1} was performed to investigate the stability of electrodes and the test results are shown in Fig. 7b. We can see that PPy/PSS-lCNT electrodes show the smoother decline trend than that of PPy/PSS-sCNT electrodes, and PPy/PSS-lCNT electrodes retain 94.0% of the initial capacitance after 5000CV cycles while PPy/PSS-sCNT electrodes keep 91.3%, this result indicates the PPy/PSS-lCNT electrodes have the relatively better cycle stability. It is well known that conducting polymer commonly suffers from a poor cyclic stability owing to the degradation caused by the swelling and shrinking of CPs [19,39]. The improved stability of composites can be ascribed to the CNT incorporated enhances the mechanical strength of composites and prevents the CPs from swelling and shrinking during the cycles. Moreover, compared with the short CNT-doped PPy/PSS-sCNT electrodes, the more superior capacitive behavior and stability for the long CNT-doped PPy/PSS-lCNT electrodes can be attributed to the more porous microstructure and the presence of a large amount of CNT within the composites, in which these long tangled CNT form an interconnected conductive nano-network for the more efficient charge transfer.

4. Conclusions

We have prepared PPy/PSS-CNT composite electrodes with an in situ electrochemically polymerized method with long and short CNT. The electrochemical measurements indicate the capacitive performance of PPy-based electrodes is significantly improved as the incorporation of CNT. Compared with the short CNT-incorporated PPy/PSS-sCNT electrodes, the long CNT-incorporated PPy/PSS-lCNT electrodes show the relatively more superior capacitive behavior and cycle stability, thereinto, the PPy/PSS-lCNT electrodes exhibit a relatively high areal capacitance of 146.1 mF cm^{-2} at 10 mV s^{-1} and retain 94.0% of the initial capacitance after 5000 CV cycles. These can be attributed to the porous surface morphology, core–shell nanostructure, and interconnected conductive nano-network due to the incorporation of a large amount of long CNT. This research demonstrates a feasible and efficient way to construct PPy/PSS-CNT nanocomposites for the increasing demands on the high-performance electrochemical energy storage devices.

Acknowledgments

References

[1] P. Simon, Y. Gogotsi, B. Dunn, Where do batteries end and supercapacitors begin? Science 343 (2014) 1210–1211.
[2] J. Liu, Charging graphene for energy, Nat. Nanotechnol. 9 (2014) 739–741.
[3] R.Z. Ma, X.H. Liu, J.B. Liang, Y. Bando, T. Sasaki, Molecular-scale heteroassembly of redoxable hydroxide nanosheets and conductive graphene into superlattice composites for high-performance supercapacitors, Adv. Mater. 26 (2014) 4173–4178.
[4] J.W. Zhao, J. Chen, S.M. Xu, M.F. Shao, Q. Zhang, F. Wei, J. Ma, M. Wei, D.G. Evans, X. Duan, Hierarchical NiMn layered double hydroxide/carbon nanotubes architecture with superb energy density for flexible supercapacitors, Adv. Funct. Mater. 24 (2014) 2938–2946.
[5] Y. Zhao, Y.N. Meng, P. Jiang, Carbon@MnO$_2$ core–shell nanospheres for flexible high-performance supercapacitor electrode materials, J. Power Sources 259 (2014) 219–226.
[6] Q.Q. Zhou, Y.R. Li, L. Huang, C. Li, G.Q. Shi, Three-dimensional porous graphene/polyaniline composites for high-rate electrochemical capacitors, J. Mater. Chem. A 2 (2014) 17489–17494.
[7] T. Zhou, Y. Qin, J. Xu, Y.X. Tao, M.H. Lu, Y. Kong, Zinc ions doped poly(aniline-co-m-aminophenol) for high-performance supercapacitor, Synth. Met. 199 (2015) 169–173.
[8] Y.W. Zhu, S. Murali, M.D. Stoller, K.J. Ganesh, W.W. Cai, P.J. Ferreira, A. Pirkle, R.M. Wallace, K.A. Cychosz, M. Thommes, D. Su, E.A. Stach, R.S. Ruoff, Carbon-based supercapacitors produced by activation of graphene, Science 332 (2011) 1537–1541.
[9] J.W. Park, S.J. Park, O.S. Kwon, C. Lee, J. Jang, J. Jang, J.W. Park, S.J. Park, C. Lee, O.S. Kwon, In situ synthesis of graphene/polyselenophene nanohybrid materials as highly flexible energy storage electrodes, Chem. Mater. 26 (2014) 2354–2360.
[10] C. Xia, Y.B. Xie, W. Wang, H.X. Du, Fabrication and electrochemical capacitance of polyaniline/titaniumnitride core–shell nanowire arrays, Synth. Met. 192 (2014) 93–100.
[11] Q. Lu, J.G.G. Chen, J.Q. Xiao, Nanostructured electrodes for high-performance pseudocapacitors, Angew. Chem. Int. Ed. 52 (2013) 1882–1889.
[12] G.S. Gund, D.P. Dubal, S.S. Shinde, C.D. Lokhande, Architectured morphologies of chemically prepared NiO/MWCNTs nanohybrid thin films for high performance supercapacitors, ACS Appl. Mater. Interfaces 6 (2014) 3176–3188.
[13] K.W. Shen, F. Ran, Y.T. Tan, X.Q. Niu, H.L. Fan, K. Yan, L.B. Kong, L. Kang, Toward interconnected hierarchical porous structure via chemical depositing organic nano-polyaniline on inorganic carbon scaffold for supercapacitor, Synth. Met. 199 (2015) 205–213.
[14] L. Chen, C.Z. Yuan, H. Dou, B. Gao, S.Y. Chen, X.G. Zhang, Synthesis and electrochemical capacitance of core–shell poly (3,4-ethylenedioxythiophene)/poly (sodium 4-styrenesulfonate)-modified multiwalled carbon nanotube nanocomposites, Electrochim. Acta 54 (2009) 2335–2341.
[15] J. Chen, C.Y. Jia, Z.Q. Wan, Novel hybrid nanocomposite based on poly(3,4-ethylenedioxythiophene)/multiwalled carbon nanotubes/graphene as electrode material for supercapacitor, Synth. Met. 189 (2014) 69–76.
[16] W.J. Chen, Y.M. He, X.D. Li, J.Y. Zhou, Z.X. Zhang, C.H. Zhao, C.S. Gong, S.K. Li, X.J. Pan, E.Q. Xie, Facilitated charge transport in ternary interconnected electrodes for flexible supercapacitors with excellent power characteristics, Nanoscale 5 (2013) 11733–11741.
[17] P. Simon, Y. Gogotsi, Materials for electrochemical capacitors, Nat. Mater. 7 (2008) 845–854.
[18] C. Li, H. Bai, G.Q. Shi, Conducting polymer nanomaterials: electrosynthesis and applications, Chem. Soc. Rev. 38 (2009) 2397–2409.
[19] S. Sahoo, S. Dhibar, G. Hatui, P. Bhattacharya, C.K. Das, Graphene/polypyrrole nanofiber nanocomposite as electrode material for electrochemical supercapacitor, Polymer 54 (2013) 1033–1042.
[20] A. Achour, J.B. Ducros, R.L. Porto, M. Boujtita, E. Gautron, L. Brizoual, M.A. Djouadi, T. Brousse, Hierarchical nanocomposite electrodes based on titanium nitride and carbon nanotubes for micro-supercapacitors, Nano Energy 7 (2014) 104–113.
[21] K. Lota, G. Lota, A. Sierczynska, I. Acznik, Carbon/polypyrrole composites for electrochemical capacitors, Synth. Met. 203 (2015) 44–48.
[22] H. Lee, H. Kim, M.S. Cho, J. Choi, Y. Lee, Fabrication of polypyrrole (PPy)/carbon nanotube (CNT) composite electrode on ceramic fabric for supercapacitor applications, Electrochim. Acta 56 (2011) 7460–7466.
[23] S. Paul, K.S. Choi, D.J. Lee, P. Sudhagar, Y.S. Kang, Factors affecting the performance of supercapacitors assembled with polypyrrole/multi-walled carbon nanotube composite electrodes, Electrochim. Acta 78 (2012) 649–655.
[24] J.Y. Kim, K.H. Kim, K.B. Kim, Fabrication and electrochemical properties of carbon nanotube/polypyrrole composite film electrodes with controlled pore size, J. Power Sources 176 (2008) 396–402.
[25] Y. Hu, Y. Zhao, Y. Li, H. Li, H.B. Shao, L.T. Qu, Defective super-long carbon nanotubes and polypyrrole composite for high-performance supercapacitor electrodes, Electrochim. Acta 66 (2012) 279–286.
[26] J.P. Liu, J. Jiang, M. Bosman, H.J. Fan, Three-dimensional tubular arrays of MnO$_2$-NiO nanoflakes with high areal pseudocapacitance, J. Mater. Chem. 22 (2012) 2419–2426.
[27] Y.Y. Horng, Y.C. Lu, Y.K. Hsu, C.C. Chen, L.C. Chen, K.H. Chen, Flexible supercapacitor based on polyaniline nanowires/carbon cloth with both high gravimetric and area-normalized capacitance, J. Power Sources 195 (2010) 4418–4422.
[28] S. Bhandari, M. Deepa, A.K. Srivastava, A.G. Joshi, R. Kant, Poly(3,4-ethylenedioxythiophene)-multiwalled carbon nanotube composite films: structure-directed amplified electrochromic response and improved redox activity, J. Phys. Chem. B 113 (2009) 9416–9428.
[29] S. Konwer, R. Boruah, S.K. Dolui, Studies on conducting polypyrrole/graphene oxide composites as supercapacitor electrode, J. Electron. Mater. 40 (2011) 2248–2255.
[30] T.M. Wu, S.H. Lin, Synthesis, characterization, and electrical properties of polypyrrole/multiwalled carbon nanotube composites, J. Polym. Sci. A: Polym. Chem. 44 (2006) 6449–6457.
[31] F.F. Liu, G.Y. Han, Y.Z. Chang, D.Y. Fu, Y.P. Li, M.Y. Li, Fabrication of carbon nanotubes/polypyrrole/carbon nanotubes/melamine foam for supercapacitor, J. Appl. Polym. Sci. 131 (2014) , doi:http://dx.doi.org/10.1002/app.39779.
[32] H.G. Wei, J.H. Zhu, S.J. Wu, S.Y. Wei, Z.H. Guo, Electrochromic polyaniline/graphite oxide nanocomposites with endured electrochemical energy storage, Polymer 54 (2013) 1820–1831.
[33] M.H. Yu, Y.X. Zeng, C. Zhang, X.H. Lu, C.H. Zeng, C.Z. Yao, Y.Y. Yang, Y.X. Tong, Titanium dioxide@polypyrrole core–shell nanowires for all solid-state flexible supercapacitors, Nanoscale 5 (2013) 10806–10810.
[34] C. Peng, J. Jin, G.Z. Chen, A comparative study on electrochemical co-deposition and capacitance of composite films of conducting polymers and carbon nanotubes, Electrochim. Acta 53 (2007) 525–537.
[35] Y.Q. Han, B. Ding, H. Tong, X.G. Zhang, Capacitance properties of graphite oxide/poly(3,4-ethylenedioxythiophene) composites, J. Appl. Polym. Sci. 121 (2011) 892–898.
[36] H.Y. Mi, X.G. Zhang, X.G. Ye, S.D. Yang, Preparation and enhanced capacitance of core–shell polypyrrole/polyaniline composite electrode for supercapacitors, J. Power Sources 176 (2008) 403–409.
[37] H. Zhao, G.Y. Han, Y.Z. Chang, M.Y. Li, Y.P. Li, The capacitive properties of amorphous manganese dioxide electrodeposited on different thermally-treated carbon papers, Electrochim. Acta 91 (2013) 50–57.
[38] H.H. Zhou, G.Y. Han, D.Y. Fu, Y.Z. Chang, Y.M. Xiao, H.J. Zhai, Petal-shaped poly (3,4-ethylenedioxythiophene)/sodium dodecyl sulfate-graphene oxide intercalation composites for high-performance electrochemical energy storage, J. Power Sources 272 (2014) 203–210.
[39] J.Y. Huang, K. Wang, Z.X. Wei, Conducting polymer nanowire arrays with enhanced electrochemical performance, J. Mater. Chem. 20 (2010) 1117–1121.